LETTERS
PUBLISHED ONLINE: 19 DECEMBER 2010 | DOI: 10.1038/NMAT2919
nature materials

Room-temperature sub-diffraction-limited plasmon laser by total internal reflection

Ren-Min Ma[1†], Rupert F. Oulton[1†], Volker J. Sorger[1], Guy Bartal[1] and Xiang Zhang[1,2*]

Plasmon lasers are a new class of coherent optical amplifiers that generate and sustain light well below its diffraction limit[1–4]. Their intense, coherent and confined optical fields can enhance significantly light–matter interactions and bring fundamentally new capabilities to bio-sensing, data storage, photolithography and optical communications[5–11]. However, metallic plasmon laser cavities generally exhibit both high metal and radiation losses, limiting the operation of plasmon lasers to cryogenic temperatures, where sufficient gain can be attained. Here, we present a room-temperature semiconductor sub-diffraction-limited laser by adopting total internal reflection of surface plasmons to mitigate the radiation loss, while using hybrid semiconductor–insulator–metal nanosquares for strong confinement with low metal loss. High cavity quality factors, approaching 100, along with strong $\lambda/20$ mode confinement, lead to enhancements of spontaneous emission rate by up to 18-fold. By controlling the structural geometry we reduce the number of cavity modes to achieve single-mode lasing.

Lasers are ideal for optical communications, information storage, accurate metrologies and sensitive spectroscopies as they present the means to deliver powerful, coherent and directional high-frequency electromagnetic energy. However, the diffraction limit of light imposes fundamental constraints on how compact such photonic devices can be and their potential for integration with electronic circuits, which are orders of magnitude smaller. Although recent efforts in photonic-crystal, whispering-gallery and metal-coated photonic cavities have succeeded in confining light to less than the vacuum wavelength, they remain limited by diffraction[12–16]. On the other hand, surface plasmon polaritons (SPPs; ref. 17), the collective electronic oscillations of metal–dielectric interfaces, show great promise for an exciting new class of light source capable of reconciling photonic and electronic length scales. Furthermore, SPPs are capable of extremely strong confinement in one or two dimensions[2,4,18,19], enabling plasmon lasers to deliver intense, coherent and directional optical energy well below the diffraction barrier. Such lasers can drastically accelerate the scalability of photonics to catch up with Moore's law for electronics and will naturally introduce new functionalities and applications. Notwithstanding the growing body of work on metal-based lasers, the demonstration of sub-diffraction-limited semiconductor plasmon lasers operating at room temperature remains a main hurdle owing to the problem of mitigating both the high absorptive loss of metals and the low cavity feedback of propagating surface plasmons in small metallic structures. This has restricted such lasers to working at cryogenic temperatures to attain sufficient gain[2,4]. Recent efforts in semiconductor plasmon lasers were only able to partially tackle these obstacles and the design stratagems remain mutually exclusive: improved feedback was obtained in devices capped in metal at the expense of high metal loss resulting in limited mode confinement[2], whereas nanowire lasers on planar metal substrates achieved reduced metal loss but had limited feedback that required cavity lengths much longer than the wavelength[4]. Room-temperature plasmon-laser operation below the diffraction limit demands effective cavity feedback, low metal loss and high gain: all within a single nanoscale device.

Here, we report the first realization of a semiconductor plasmon laser operating at room temperature with $\lambda/20$ optical confinement. A 45-nm-thick cadmium sulphide (CdS) nanosquare atop a silver surface separated by a 5-nm-thick magnesium fluoride gap layer provides the sub-diffraction-limited mode confinement and low metal loss[20]. Surprisingly, although the high-index material is only 45 nm thick, the surface plasmons of this system carry high momentum, even higher than light waves in bulk CdS or plasmonic nanowire lasers[4]. This leads to strong feedback by total internal reflection of surface plasmons at the cavity boundaries.

Figure 1a,b shows a schematic diagram of the room-temperature plasmon laser and a scanning electron microscopy (SEM) micrograph of the 45-nm-thick, 1-μm-length square plasmon laser sitting atop a silver substrate with a 5 nm MgF_2 gap, respectively. The close proximity of the high-permittivity CdS square and silver surface enables modes of the CdS square to hybridize with SPPs of the metal–dielectric interface, leading to strong confinement of light in the gap region (Fig. 1c) with relatively low metal loss[20]. The coupling is extremely strong and causes a dramatic increase in the momentum with respect to the modes of the CdS square alone (blue arrow in Fig. 1d). As the dominant magnetic-field component of the waves is always parallel to the metal surface, we call these transverse magnetic (TM) waves (the convention in this letter differs from the TM-wave definition with respect to the dielectric–air interface where the total internal reflection takes place). On the other hand, waves with dominant electric field parallel to the metal surface (transverse electric or TE) cannot hybridize with SPPs. Consequently, they become increasingly delocalized as the gap size decreases and are effectively pushed away from the metal surface (Fig. 1c) with a corresponding decrease in momentum with respect to TE waves of the CdS square alone (red arrow in Fig. 1d). Although both wave polarizations are free to propagate in the plane, only TM waves have sufficient momentum to undergo total internal reflection and achieve the necessary feedback for lasing as shown in Fig. 1e (refs 21,22). Although CdS squares thicker than about 60 nm can support TE waves with sufficient momentum to undergo total internal reflection, they are scattered out of the plane more effectively than TM waves because they are delocalized from the metal surface. Although long-lived eigenmodes of square cavities are achievable[23], the finite size of the cavity leads to imperfect internal reflection causing in-plane scattering of surface plasmon waves and

[1]NSF Nanoscale Science and Engineering Centre, 3112 Etcheverry Hall, University of California, Berkeley, California 94720, USA, [2]Materials Sciences Division, Lawrence Berkeley National Laboratory, 1 Cyclotron Road, Berkeley, California 94720, USA. †These authors contributed equally to this work.
*e-mail: xiang@berkeley.edu.

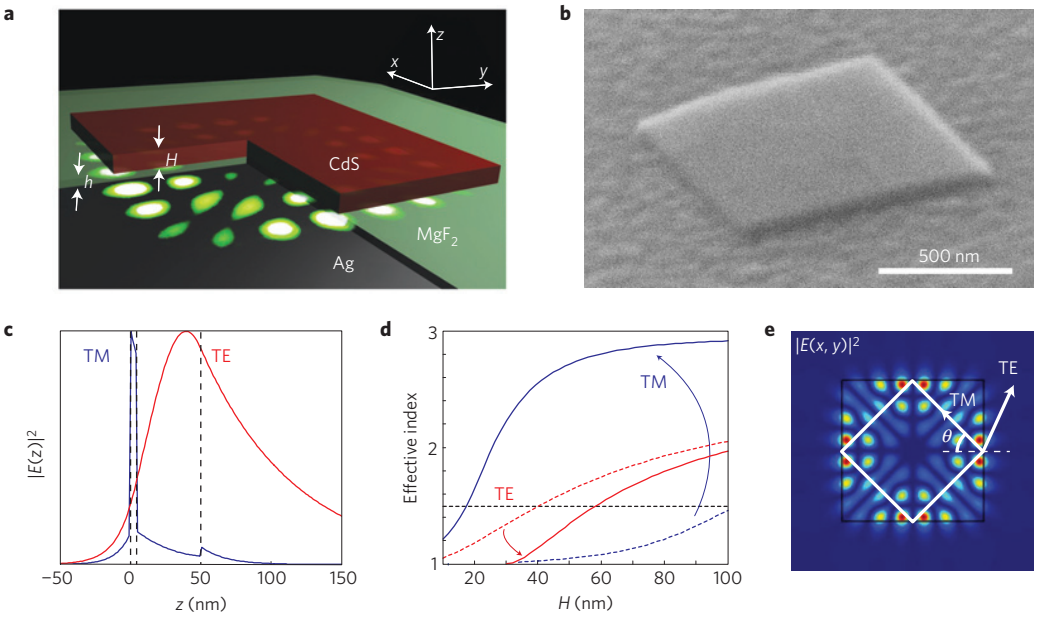

Figure 1 | The room-temperature plasmon laser. a, Schematic diagram of the room-temperature plasmon laser showing a thin CdS square atop a silver substrate separated by a 5 nm MgF_2 gap, where the most intense electric fields of the device reside. **b**, SEM micrograph of the 45-nm-thick, 1-μm-length CdS square plasmon laser studied here. **c**, The electric-field-intensity distribution of the two modes of the system along the *z* direction. Although TM modes are localized in the gap layer, TE modes are delocalized from the metal surface. **d**, The effective index of TM and TE waves with (solid line) and without (dashed line) the metal substrate. TM waves strongly hybridize with SPPs resulting in strong confinement within the gap region (blue line in **c**) accompanied by a dramatic increase in momentum (blue line in **d**) with respect to TM waves of the CdS square alone (blue dashed line in **d**). However, the delocalized TE waves (red line in **c**) show decreased momentum (red line in **d**) with respect to TE waves of the CdS square alone (red dashed line in **d**). **e**, Electric-field-intensity distribution of a TM mode in the *x* and *y* directions. Although both mode polarizations are free to propagate in the plane, only TM modes have sufficiently large mode index to undergo efficient total internal reflection, providing the feedback for lasing.

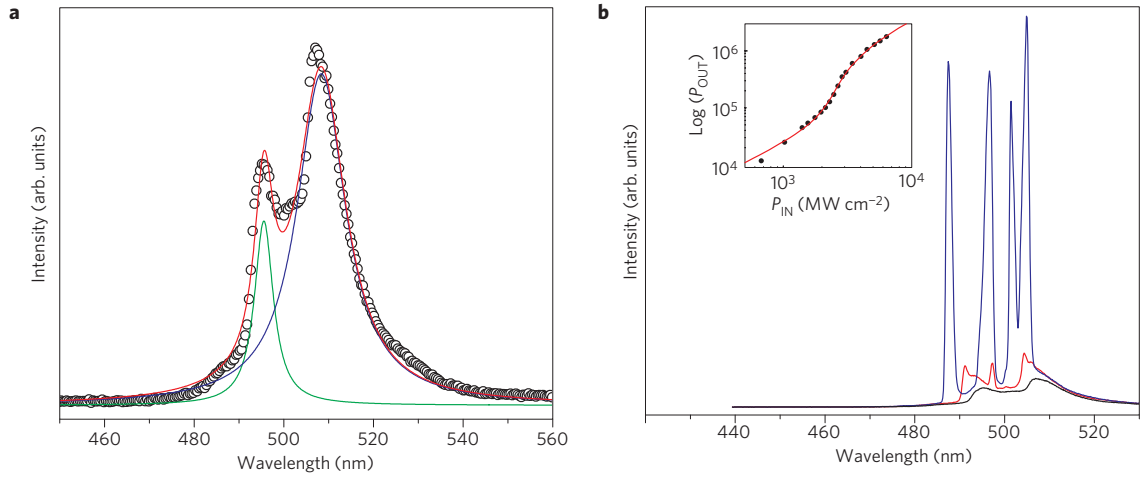

Figure 2 | Laser spectra and integrated light-pump response of a room-temperature plasmon laser below and above threshold. a, The spontaneous emission spectrum at a peak pump intensity of 1,960 MW cm^{-2} shows obvious cavity modes despite being below the threshold, which indicates the excellent cavity feedback. **b**, Room-temperature laser spectra and integrated light-pump response (inset) showing the transition from spontaneous emission (1,960 MW cm^{-2}, black) through amplified spontaneous emission (2,300 MW cm^{-2}, red) to full laser oscillation (3,074 MW cm^{-2}, blue).

volume scattering of radiation waves, which we use to measure the response of the plasmon laser (see Supplementary Information).

The feedback mechanism of totally internally reflected SPPs is extremely effective, as shown by the well-pronounced cavity modes in the spontaneous emission spectrum below the threshold (see Supplementary Information) in Fig. 2a. The *Q* factors of the two apparent modes are 97 and 38 at the resonant wavelengths of 495.5 nm and 508.4 nm, respectively. We have identified these as plasmonic total-internal-reflection modes using a numerical model (see Supplementary Information). Although the *Q* of the 495.5 nm resonance is close to numerical predictions, the other *Q* value is an underestimate because that resonance is composed of several modes that are too close to be resolved. For larger pump intensities, multiple cavity modes appear with orders-of-magnitude-higher coherence than the underlying spontaneous emission, as shown in Fig. 2b. The emission spectrum is completely dominated by these high-coherence peaks when collecting the light at large collection angles, because the plasmonic cavity modes preferentially scatter into large angles to conserve their in-plane momentum (see Supplementary Information). The nonlinear response of

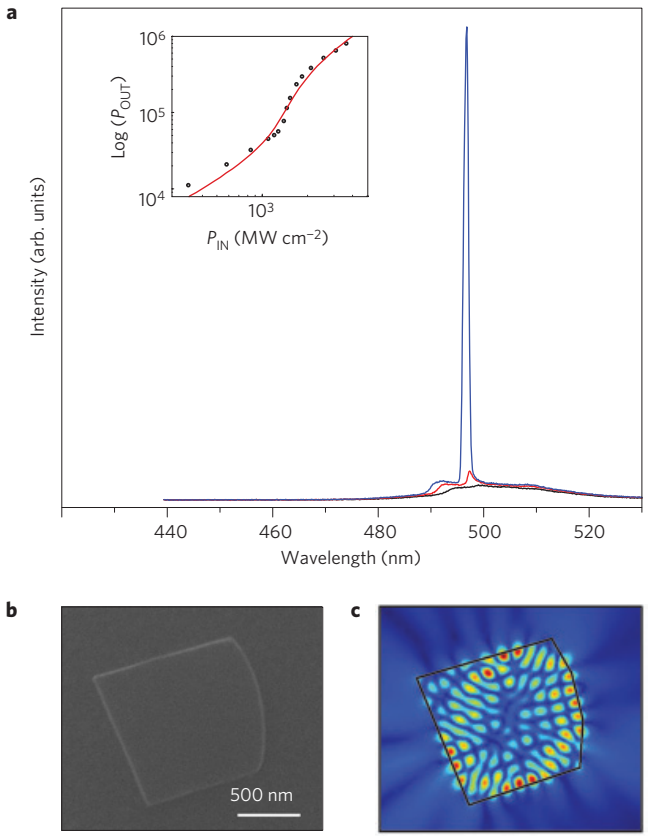

Figure 3 | Laser spectrum and integrated light-pump response of a single-mode room-temperature plasmon laser. a, The room-temperature laser spectra and integrated light-pump response (inset) showing the transition from spontaneous emission (1,096 MW cm^{-2}, black) through amplified spontaneous emission (1,280 MW cm^{-2}, red) to full single-mode laser oscillation (1,459 MW cm^{-2}, blue) and the spectral narrowing of the single laser mode. **b**, The SEM micrograph of the device. The curved facet breaks the four-fold symmetry and thereby inhibits high-order modes that exist in the square CdS lasers. **c**, The electric-field-intensity distribution of the lasing mode (see Supplementary Information).

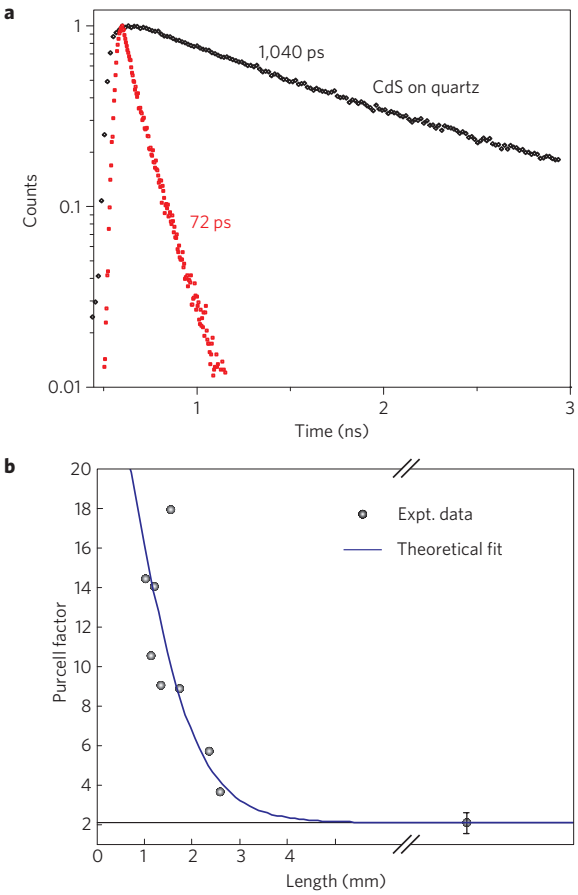

Figure 4 | Observation of the Purcell effect. a, Time-resolved spontaneous emission under weak pumping conditions shows a dramatic reduction in lifetime compared with CdS on quartz. The combination of high cavity quality and strong confinement enhances the spontaneous emission rate 14-fold, owing to the Purcell effect[24]. The lifetime is measured for the same device as presented in Fig. 1b. **b**, The increase in Purcell effect with the decrease of the cavity side length as a result of the mode volume reduction accompanied by a high quality factor. Very large cavities do not benefit from cavity feedback and exhibit a Purcell effect of two (the rightmost point, with error bar showing standard deviation) owing to confinement along the *z* direction alone. This agrees well with a simple theoretical model taking into account the numerous emission processes (see Methods). This indicates the ability of these plasmon lasers to strongly enhance light–matter interactions. The variations in the CdS thickness (45–88 nm) do not play a main role in the emission enhancement.

the integrated output power to pump intensity confirms the observation of laser oscillation well above threshold (inset of Fig. 2). This laser can be considered to be a SPASER (surface plasmons amplified by stimulated emission of radiation) as originally introduced in ref. 1, since it generates plasmonic cavity eigenmodes and only emits light to the far-field as a side-effect of scattering.

The current device exhibits multiple laser peaks attributed to the number of available modes in the square cavity configuration (see Supplementary Information). However, we have also observed single-mode plasmon lasing in irregularly shaped devices with lower symmetry where only a limited number of modes can undergo total internal reflection. Figure 3 shows the spectrum and power response of a single-mode room-temperature plasmon laser along with a SEM micrograph of the device with 75 nm thickness and 1.1 μm length in Fig. 3b. Lasing in such ultrathin devices is viable solely owing to the plasmonic confinement and strong total-internal-reflection feedback. This was verified from control samples, consisting of similar CdS squares on quartz substrates: none exhibited laser action owing to the lack of both mode confinement and cavity feedback.

The intense fields that are generated and sustained in the gap region (Fig. 1c) make such lasers highly useful for investigating light–matter interactions. Namely, an emitter placed in this gap region is expected to interact strongly with the laser light. Such light–matter interaction enhancements are also observable to a lesser extent in the CdS gain medium; under weak pumping, the CdS band-edge transitions of this plasmon laser (device shown in Fig. 1b) show a spontaneous emission lifetime reduced by a factor of 14 (Fig. 4a). The Purcell effect[24] is apparent in all the laser devices measured, as shown in Fig. 4b. We note that in this work we sacrifice the lateral confinement achievable in plasmonic nanowire lasers[4], and use surface-plasmon total internal reflection to realize a three-dimensional cavity with strong feedback. It is this combination of both high cavity quality factors (Q) and strong mode confinement that leads to Purcell factors as large as 18 in smaller devices. On the other hand, for devices larger than the surface-plasmon propagation length, the cavity feedback no longer plays a role and an average twofold reduction in lifetime is obtained owing to the strong confinement of SPPs alone. A theoretical formula describing the observed lifetime reduction is shown in Fig. 4b and predicts SPP losses of 6,323 cm^{-1}, in good

agreement with the numerical estimate (see Methods). We note that this plasmon loss can be compensated by gain available in CdS (ref. 25). Since the electric-field intensities in the gap region are five times stronger than in the CdS, we anticipate Purcell factors as high as 90 for light–matter interactions within the gap. Despite sub-diffraction-limited confinement in only one dimension, this value is even higher than the highest simulated Purcell factors of 60 for the recently reported metal-coated photonic cavities[14–16].

We have demonstrated room-temperature semiconductor plasmon lasers with strong mode confinement, which are also much smaller than the diffraction limit. The mode is generated inside a nanoscopic gap layer of 5 nm and remains bound by strong feedback arising from total internal reflection of surface plasmons. The small mode size and high quality factor give rise to a strong Purcell effect, resulting in an up-to-18-fold enhancement of the natural spontaneous emission rate of CdS band-edge transitions. This indicates that these sub-diffraction-limited laser modes have the potential to enhance light–matter interactions. Room-temperature plasmon lasers enable new possibilities in applications such as single-molecule sensing, ultrahigh-density data storage, nanolithography and optical communications.

Methods

Device fabrication and experiment set-up. The CdS squares were made by a solution-based sonication cleaving process of CdS nanobelts, which were synthesized through the chemical vapour deposition method[26]. The squares were then deposited from solution on MgF_2/Ag (5 nm/300 nm) substrates. A frequency-doubled, mode-locked Ti–sapphire laser (Spectra Physics) was used to pump the squares ($\lambda_{pump} = 405$ nm, repetition rate 10 kHz, pulse length 100 fs). A ×20 objective lens (numerical aperture = 0.4) focused the pump beam to a ~ 5-μm-diameter spot on the sample. All experiments were carried out at room temperature.

Theoretical Purcell factor. We compare the measured Purcell factors of a number of lasers with a theoretical model in Fig. 4b. For very large cavities, we expect an enhanced emission rate γ_{SP} with respect to the usual rate of CdS band edge transitions, γ_0, owing to strong TM-wave confinement. On reducing the cavity size, it can be shown that the feedback increases the emission rate to $\gamma \cong \gamma_{SP} + \bar{Q}B$ where $\bar{Q} = m\pi e^{-\alpha\bar{L}}/(1 - e^{-2\alpha\bar{L}})$ is the averaged cavity-mode quality factor, m is the average mode order, α is the round-trip cavity loss, $\bar{L}$ is the average round-trip path of a TM cavity mode within a CdS square and B is an unknown factor that depends on the average number of cavity modes and their average mode volume within the CdS emission bandwidth. To facilitate a numerical comparison of this formula with the experimental data, we have derived the basic functional form, $B = \beta L$, and assume that $\bar{L} = L/\sqrt{2}$ is the minimum round-trip cavity length (see Supplementary Information). The Purcell factor, $F = \gamma/\gamma_0 \cong F_\infty[1 + \beta L \mathrm{csch}(\alpha L/\sqrt{2})]$, where F_∞ is the known enhancement factor for large cavities, and α and β are unknowns. The least squares fit in Fig. 4b gives $\alpha = 6{,}323\ \mathrm{cm}^{-1}$, $\beta = 4.93$ and $F_\infty = 2.08$.

Received 28 June 2010; accepted 3 November 2010; published online 19 December 2010

References

1. Bergman, D. J. & Stockman, M. I. Surface plasmon amplification by stimulated emission of radiation: Quantum generation of coherent surface plasmons in nanosystems. *Phys. Rev. Lett.* **90,** 027402 (2003).
2. Hill, M T. *et al.* Lasing in metal–insulator–metal sub-wavelength plasmonic waveguides. *Opt. Express* **17,** 11107–11112 (2009).
3. Noginov, M. A. *et al.* Demonstration of a spaser-based nanolaser. *Nature* **460,** 1110–1113 (2009).
4. Oulton, R. F. *et al.* Plasmon lasers at deep subwavelength scale. *Nature* **461,** 629–632 (2009).
5. Schuller, J. A. *et al.* Plasmonics for extreme light concentration and manipulation. *Nature Mater.* **9,** 193–204 (2010).
6. Gramotnev, D. K. & Bozhevolnyi, S. I. Plasmonics beyond the diffraction limit. *Nature Photon.* **4,** 83–91 (2010).
7. Anker, J. N. *et al.* Biosensing with plasmonic nanosensors. *Nature Mater.* **7,** 442–453 (2008).
8. Dionne, J. A., Diest, K., Sweatlock, L. A. & Atwater, H. A. PlasMOStor: A metal–oxide–Si field effect plasmonic modulator. *Nano Lett.* **9,** 897–902 (2009).
9. Zijlstra, P., Chon, J. W. M. & Gu, M. Five-dimensional optical recording mediated by surface plasmons in gold nanorods. *Nature* **459,** 410–413 (2009).
10. Challener, W. A. *et al.* Heat-assisted magnetic recording by a near-field transducer with efficient optical energy transfer. *Nature Photon.* **3,** 220–224 (2009).
11. Stipe, B. C. *et al.* Magnetic recording at 1.5 Pb m^{-2} using an integrated plasmonic antenna. *Nature Photon.* **4,** 484–488 (2010).
12. Altug, H., Englund, D. & Vuckovic, J. Ultrafast photonic crystal nanocavity laser. *Nature Phys.* **2,** 484–488 (2006).
13. Song, Q., Cao, H., Ho, S. T. & Solomon, G. S. Near-IR subwavelength microdisk lasers. *Appl. Phys. Lett.* **94,** 061109 (2009).
14. Hill, M. T. *et al.* Lasing in metallic-coated nanocavities. *Nature Photon.* **1,** 589–594 (2007).
15. Nezhad, M. P. *et al.* Room-temperature subwavelength metallo-dielectric lasers. *Nature Photon.* **4,** 395–399 (2010).
16. Yu, K., Lakhani, A. & Wu, M. C. Subwavelength metal-optic semiconductor nanopatch lasers. *Opt. Express* **18,** 8790–8799 (2010).
17. Maier, S. A. *Plasmonics: Fundamentals and Applications* (Springer, 2007).
18. Akimov, A. V. *et al.* Generation of single optical plasmons in metallic nanowires coupled to quantum dots. *Nature* **450,** 402–406 (2007).
19. Kolesov, R. *et al.* Wave–particle duality of single surface plasmon polaritons. *Nature Phys.* **5,** 470–474 (2009).
20. Oulton, R. F., Sorger, V. J., Genov, D. A., Pile, D. F. P. & Zhang, X. A hybrid plasmonic waveguide for subwavelength confinement and long-range propagation. *Nature Photon.* **2,** 496–500 (2008).
21. Poon, A. W., Courvoisier, F. & Chang, R. K. Multimode resonances in square-shaped optical microcavities. *Opt. Lett.* **26,** 632–634 (2001).
22. Huang, Y-Z., Chen, Q., Guo, W-H. & Yu, L-J. Experimental observation of resonant modes in GaInAsP microsquare resonators. *IEEE Photonics Technol. Lett.* **17,** 2589–2591 (2005).
23. Wiersig, J. Formation of long-lived, scarlike modes near avoided resonance crossings in optical microcavities. *Phys. Rev. Lett.* **97,** 253901 (2006).
24. Purcell, E. M. Spontaneous emission probabilities at radio frequencies. *Phys. Rev.* **69,** 681 (1946).
25. Ninomiya, S. & Adachi, S. Optical properties of wurtzite CdS. *J. Appl. Phys.* **78,** 1183–1190 (1995).
26. Ma, R-M., Dai, L. & Qin, G-G. High-performance nano-Schottky diodes and nano-MESFETs made on single CdS nanobelts. *Nano Lett.* **7,** 868–873 (2007).

Acknowledgements

The authors thank X. B. Yin for discussions. We acknowledge financial support from the US Air Force Office of Scientific Research (AFOSR) MURI program under grant no. FA9550-04-1-0434 and by the National Science Foundation Nano-Scale Science and Engineering Center (NSF-NSEC) under award CMMI-0751621.

Author contributions

R-M.M., R.F.O. and X.Z. developed the device concept and design. R-M.M., R.F.O. and V.J.S. carried out the experiments. R.F.O. and R-M.M. conducted theoretical simulations. R-M.M., R.F.O., G.B. and X.Z. discussed the results and wrote the manuscript.

Additional information

The authors declare no competing financial interests. Supplementary information accompanies this paper on www.nature.com/naturematerials. Reprints and permissions information is available online at http://npg.nature.com/reprintsandpermissions. Correspondence and requests for materials should be addressed to X.Z.